HEFAT 2012
9th International Conference on Heat Transfer, Fluid Mechanics and Thermodynamics
July 16-18, 2012
Malta

CFD ANALYSIS FOR SOLAR CHIMNEY POWER PLANTS

Hermann Fasel *, Ehsan Shams, Andreas Gross
Aerospace and Mechanical Engineering Department
University of Arizona
Tucson, Arizona 85721

ABSTRACT

Computational Fluid Dynamics (CFD) was employed for investigating Solar Chimney Power Plants (SCPP). The effect of the geometric dimensions on the fluid dynamics and heat transfer was investigated. The thermal efficiency of the collector was found to improve with increasing scale, due to an increase of the heat transfer coefficient. The spread in relevant Reynolds numbers for the collector and chimney was four orders of magnitude from the smallest to the largest scale. Parametric studies were also performed to determine the effect of the distance of the collector from the ground on the power output. An optimum distance was determined for two different scales.

NOMENCLATURE

A	$[m^2]$	area
c_p	$[J/kgK]$	specific heat capacity
D	[m]	chimney diamter
g	$[m/s^2]$	gravitational acceleration
h	$[W/m^2K]$	convective heat transfer coefficient
H	[m]	collector height
H_T	[m]	tower height
I	$[W/m^2]$	solar irradiation
K	[W/mK]	thermal conductivity
$\dot{m}$	[kg/s]	mass flux
N	[W]	power
Nu		Nusselt Number
p	$[N/m^2]$	pressure
q''	$[W/m^2]$	heat flux
R	[m]	collector radius
Re		Reynolds number
T	[K]	temperature
U	[m/s]	velocity
ε		emission coefficient
μ	$[Ns/m^2]$	dynamic viscosity
ρ	$[kg/m^3]$	density
σ	$[W/m^2K^4]$	Stefan-Boltzman constant
θ		dimensionless temperature

subscripts	
a	ambient
avg	average
cond	conduction
conv	convection
emis	emission
T	Tower (chimney)

INTRODUCTION

Large-scale Solar Chimney Power Plants (SCPP) are economically viable alternatives to other forms of solar energy production (1). Such plants, also often referred to as Solar Updraft Tower Plant (SUTP), could be located, for example, in the vast desert flat lands of the Southwestern United States. The operating principle of the SCPP is relatively simple: Solar radiation heats the air underneath a transparent collector (greenhouse effect). The hot air passes through turbines, which drive electrical generators, and then the air escapes through the tower (chimney effect). Figure 1 shows a schematic of a SCPP. A demonstration plant, funded by the German Ministry of Science and Technology in Manzanares (Spain) confirmed theoretical predictions based on one-dimensional fluid/thermodynamic analysis and demonstrated potential secondary uses, such as greenhouse farming. The solar-typical nighttime interruption of power production could be avoided by releasing thermal energy that was stored in the ground and/or in water tanks. This kept the plant operational even at night. However, due to the scaling effects, SCPPs have to be very large to be cost competitive (1).

*Correspondence to: faselh@email.arizona.edu

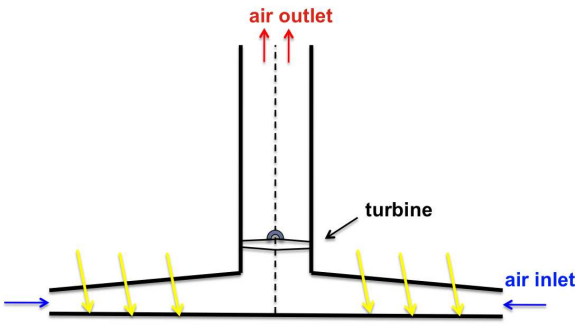

FIGURE 1. Schematic cross section of a solar chimney, showing the system elements and working principle

With projected costs of $800M to $1000M for a 200 [MW] plant and with unknown environmental and societal impact, it is understandable why power companies and financial institutions are reluctant to commit to this technology, in particular because the predicted power of such large plants is based on extrapolations from a limited set of sub-scale experiments and simplified models.

Simple models, such as energy balance models or one-dimensional fluid dynamics models (2; 3; 4) are likely not sufficient for reliable analyses of such large-scale plants. Axisymmetric or full three-dimensional Computational Fluid Dynamics (CFD) simulations based on the complete Navier-Stokes equations are required for accurate investigations of the performance of entire plants or of individual key components. Towards this end, in our research Unsteady Reynolds-Averaged Navier-Stokes (URANS) calculations were carried out using a commercially available CFD package (ANSYS Fluent). For these calculations, the heat loss into the ground and the heat release into the air underneath the collector were modeled based on an energy balance.

The main objective of our investigations was to examine the scaling effects on the coupled fluid flow and heat transfer phenomena underneath the collector, the chimney and the entire plant. The geometric scales were based on the dimensions of the Manzanares pilot plant, which had a chimney with 198m height and 10m diameter, and a collector with a 244m diameter and a 2m distance from the ground ("collector height") (5). For these scale investigations, CFD calculations were carried out where the geometric dimensions of the Manzanares plant were scaled by 1:250 (very small laboratory model), 1:30, 1:10, 1:5, 1:2, 1:1 (reference Manzanares plant), 2:1, and 5:1 (future 200MW plant). A 1:250 scale laboratory model is available at the University of Arizona and can be used for validating the CFD calculations. A fully instrumented 1:30 scale model is currently being constructed and will also be available for CFD validation.

Parametric studies were also carried out to investigate the effect of the distance between the collector and the ground ('collector height) on the power production. An optimal collector height was identified for two geometrical scales.

The paper is organized as follows: First, the computational model is introduced. Then, the approach is validated using measurement data from a laboratory scale model. Then CFD results for the various scale models are presented and discussed. Finally, a summary and some conclusions are provided.

COMPUTATIONAL MODEL

The incompressible Navier-Stokes equations and a conservation equation for the thermal energy were solved using the Ansys Fluent software. The incompressible flow assumption is justified for the SCPP application since the maximum Mach number is much smaller than 0.1. The buoyancy effects are taken into account by allowing a variation of density as a function of temperature.

The relevant Reynolds numbers for large-scale plants are far too large for resolving all scales of the turbulent fluid motion in Direct Numerical Simulations (DNS). Therefore, the Reynolds-averaged equations were solved in an unsteady fashion (Unsteady Reynolds-Averaged Navier-Stokes, URANS). The unresolved turbulence was modeled using the Fluent Reynolds Stress Model (RSM), which requires the solution of five additional transport equations (3 Reynolds stress components, turbulent kinetic energy k, and turbulent dissipation, ε). Other linear two-equation turbulence models, i.e., the $k-\varepsilon$ and $k-\omega$ model, were tested earlier but were found to be less accurate than the RSM. More details on the computational models, including the model constants, etc. are provided in Shams *et al.* (6).

For the simulations of the large-scale models (larger than 1:30 scale) the viscous sublayer was not resolved and the standard wall function by Launder and Spalding (7) was employed. For the smaller-scale models the near-wall grid resolution in wall units, y^+, was less than 1.

The SIMPLE algorithm available in the Fluent package was employed for solving the system of equations. The convective terms were discretized with a second-order-accurate upwind scheme. The higher-order-accurate QUICK scheme was tested but showed no significant improvement over the upwind scheme.

Computational Domain and Boundary Conditions

Axisymmetry was assumed for all simulations (the symmetry axis is the chimney centerline). A structured grid was employed inside the SCPP and in its immediate vicinity (Fig. 2). The ambient (outer) domain was discretized using an unstructured grid while the (inner) domain underneath the collector and in the chimney was discretized using a structured grid. The inner structured and outer unstructured grids are coupled via a non-conformal mapping algorithm. The coarse unstructured grid in the ambient allows the ambient boundary to be placed at considerable distance from the SCPP, so that the use of zero-velocity

and fixed-ambient-temperature boundary conditions is justified. The ambient domain is needed for obtaining realistic inflow and outflow boundary conditions for the collector and chimney. The heat transfer inside the tower wall and collector cover were modeled assuming a finite material thickness and material-specific heat transfer coefficients.

Figure 2 shows details of the computational grid. The overall domain dimensions are 10 times the size of the SCPP (in both the axial and radial direction). The boundaries are labeled in Figure 2(a). No-slip wall-boundary conditions were enforced at boundaries 1, 2, and 3. The symmetry axis condition was applied at boundary 4. At boundaries 2 and 3 and for the part of boundary 1 that is not underneath the collector the ambient temperature, $T_{amb} = 288$K, was prescribed. Table 1 shows the dimensions of the Manzanares pilot plant.

TABLE 1. Dimensions of Manzanares solar chimney power plant (reference scale)

	Manzanares [m]
Chimney height H_t	198
Chimney radius R_t	5
Collector height H_c	2
Collector radius R_c	122

An energy balance model was applied to determine the wall temperature on the ground underneath the collector (boundary 1, underneath collector). Figure 3 provides a schematic of the temperature distributions and heat transfer underneath the collector. The total amount of solar incidence on the ground I_{total} is divided into emission q''_{emis}, convection into the air stream underneath the collector q''_{conv}, and conduction into the ground q''_{cond},

$$I_{total} = q''_{emis} + q''_{conv} + q''_{cond}\,, \tag{1}$$

where, $q''_{conv} = -K_{air}\,dT/dy$, $q''_{cond} = -K_{ground}\,dT/dy$, and $q''_{emis} = \varepsilon\sigma T^4_{ground}$. An integral approximation exists for determining the conduction heat penetration into the ground (8). Equation 1 is solved iteratively for the ground temperature at each time step.

Verification

In order to demonstrate that the outer ambient domain was required, we performed two separate simulations, one with the outer domain and the other one without it. For the simulation without the outer domain, uniform inflow velocity with zero pressure gradient and fully developed outflow boundary condition were specified. Table 2 provides the temperature, velocity,

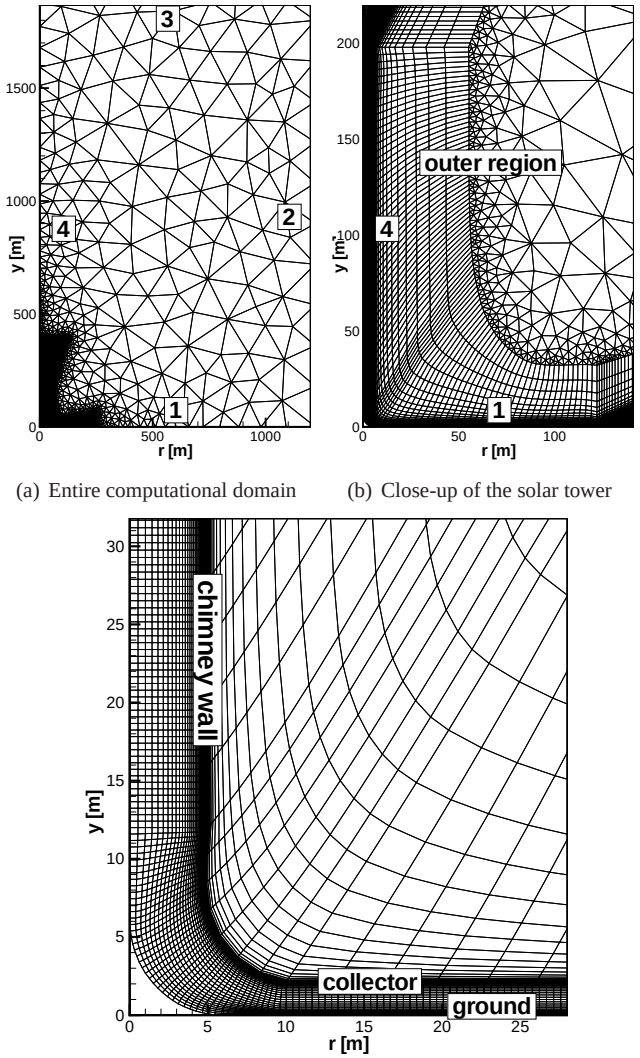

(a) Entire computational domain (b) Close-up of the solar tower

(c) Close-up of the collector and tower interfaces

FIGURE 2. Typical grid used for axisymmetric computations

and mass flow rate inside the chimney at 10% of the chimney height. Because the results show close to 10% difference in the velocity, for the extended domain, it was decided that the ambient domain had to be included despite the increased computational cost incurred by the larger domain and the slower convergence of the solution compared to the case without the ambient domain.

Validation

Measurements from a 1:250 scale laboratory model at the University of Arizona were used to validate the simulation approach (6). The radial temperature distribution of the air inside the collector (at mid-height between ground and collector cover) was measured using J-Type thermocouples. The esti-

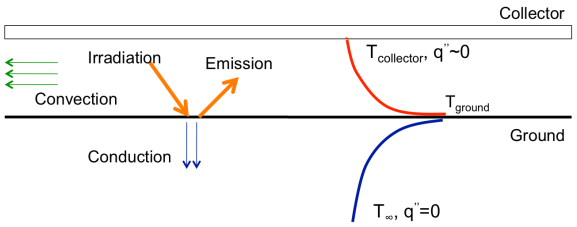

FIGURE 3. Schematic of temperature distributions and heat fluxes under the collector

		extended	not-extended	difference
T_{avg}	[K]	339.6	349.7	-2.9%
U_{avg}	[m/s]	0.690	0.763	-9.7%
mass flow rate	[g/s]	0.8057	0.8738	-7.8%

TABLE 2. Effect of domain extent on the performance of solar chimney. Data was extracted at 10% of the chimney height.

mated uncertainty of the temperature measurements was about 2%. More thermocouples were also embeded under a circular aluminum plate to measure the ground temperature. A comparison between measured and computed temperature distributions is shown in Figure 4. The simulation results obtained without turbulence model match the experimental data better, which suggests that the laminar flow assumption is justified for the very small scale. Small differences can be observed only near the tower base ($r/R_c < 0.12$).

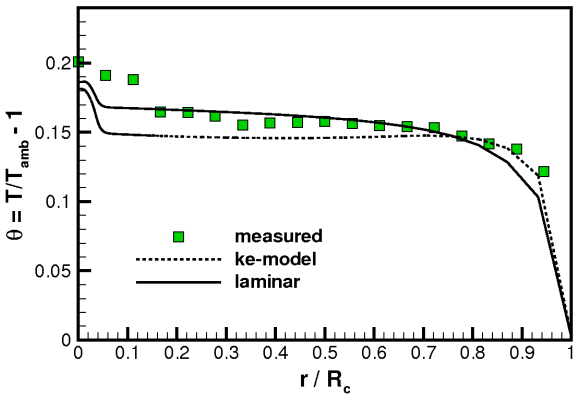

FIGURE 4. Radial temperature distribution in the collector at half the collector height for laboratory scale model; measured data (symbols), data from laminar flow simulation (solid line) and calculation with $k-\varepsilon$ model (dashed line)

For further validation a calculation with an ambient domain was carried out for the Manzanares scale SCPP (5). Contours of the velocity magnitude and temperature as well as the turbulent kinetic energy and eddy viscosity ratio are shown in Figure 5. Both turbulent kinetic energy and turbulent viscosity increase

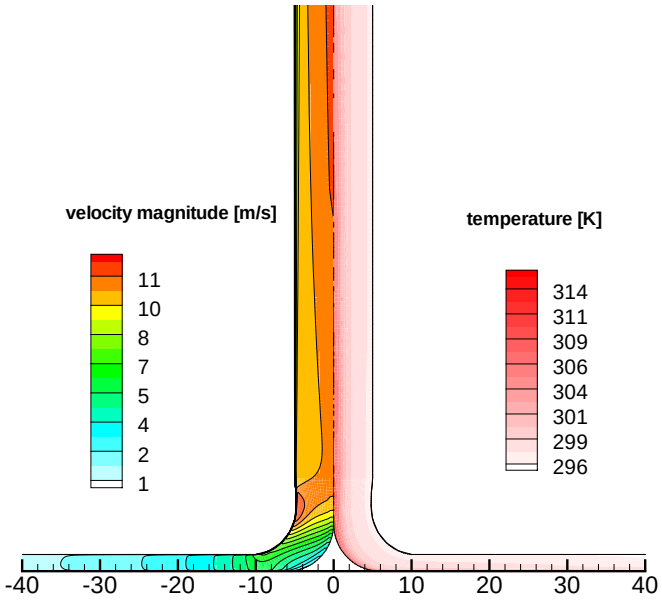

(a) Contours of velocity and temperature

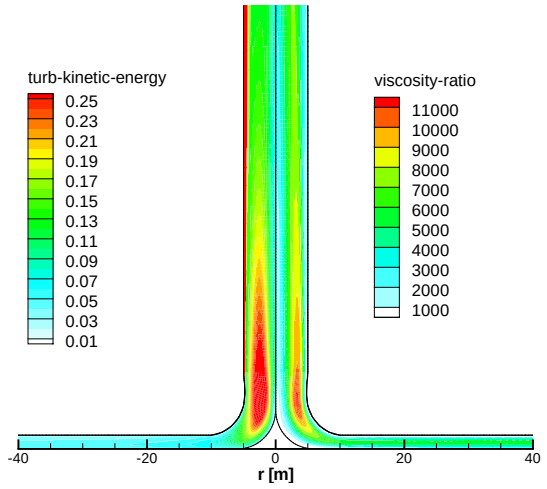

(b) Contours of turbulent kinetic energy m^2/s^2 (left) and turbulent viscosity ratio (right)

FIGURE 5. Manzanares scale

significantly at the chimney entrance section. The predicted peak velocity of U_{avg}=12m/s and the average air temperature increase of 15°C agree well with the Manzanares test data reported by Haaf (9).

SCALING EFFECT

For future SCPPs to be economical they have to be very large (chimneys as high as 1000m are being considered (1)). Simulations with SCPPs of different scales were carried out to investigate how the fluid dynamics and heat transfer were affected by the scale. The energy balance model (5) predicts that the electrical power scales with the product of chimney height, H_T, and collector area, $A_{collector} = \pi R_c^2$,

$$P = \frac{2}{3}\eta_{collector}\frac{g}{c_p T_a} I_{total} \times H_T \times A_{collector}\,, \tag{2}$$

where g is the gravitational acceleration. The main intent of the present investigation was to determine if this cubic scaling remains valid for very large scales. Simulations are carried out for scaled models of the Manzanares SCPP. The scaling factors used in these simulations are 1:250, 1:30, 1:10, 1:5, 1:2, 1:1, and 5:1.

The plant performance depends on the mass flow rate in the chimney, which is a function of the size of the SCPP as well as the temperature increase in the collector. For the purpose of this paper, the maximum available power was defined by integrating the product of dynamic pressure and velocity over a chimney cross section at 10% of the chimney height,

$$N_{max} = \int_{A_{chimney}} p_{dynamic} v \, dA. \tag{3}$$

Since, $p_{dynamic} = 1/2\rho v^2$, the available power is cubically proportional to the rising velocity. The thermal efficiency of the collector (5),

$$\eta_{collector} = \frac{\dot{m} c_p \Delta T}{I_{total} \times A_{collector}}\,, \tag{4}$$

depends on the temperature rise in the collector, which in turn is dependent on the ground heat transfer and the collector roof insulation among others, etc. Here, $\dot{m}$ is the mass flux through the plant.

The velocity at 10% of the chimney height, the mass flow rate, and available power for the different scales are shown in Figure 6. Using an energy balance (5), the velocity in the chimney can be predicted to be proportional to the square root of the tower height,

$$v = \sqrt{2 g H_T \frac{\Delta T}{T_a}}\,, \tag{5}$$

where ΔT is the temperature increase in the collector and T_a is the ambient temperature. Figure 6(a) reveals that this model is valid

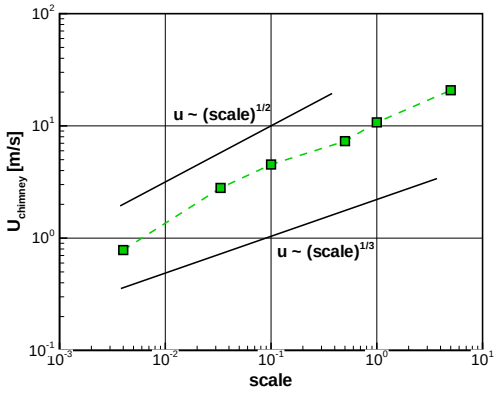

(a) Rising velocity

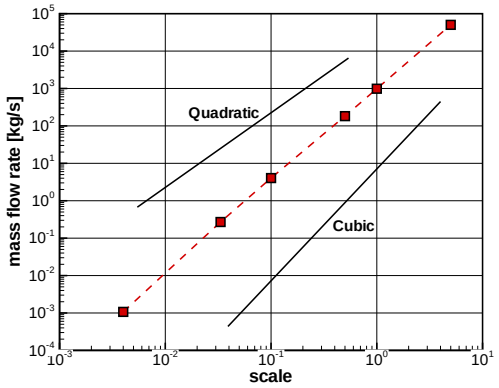

(b) Mass flow rate

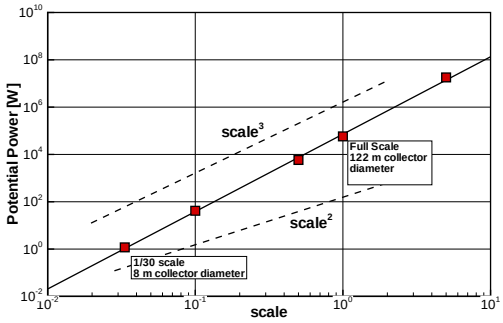

(c) Available power (see Equation 3

FIGURE 6. Solar chimney performance for different scales

over the entire range of investigated scales. The mass flow rate (Fig. 6(b)) and the available power (Fig. 6(c)), display a nearly cubic scaling with the size of the SCPP. Since the power (Eq. 3) scales with the cube of the velocity in the chimney it is also directly dependent on the tower height H_T and the temperature increase ΔT in the collector (Eq. 5).

Because the chimney constitutes one of the most expensive components of large SCPPs its height will most likely be limited in exchange for a larger collector area. When the tower height

is limited, the temperature rise ΔT has to be increased to increase the velocity in the tower. In order to better understand what factors influence the temperature increase, the heat transfer in the collector has to be investigated in more detail. Figure 7(a) shows wall-normal temperature distributions in the collector at $r = 3R_{chimney}$. In Figure 7(b) radial temperature distributions at the collector mid-height (halfway between ground and collector cover) are plotted.

Figure 7(c) displays radial temperature distributions on the ground. The ground temperature is obtained from the energy balance model, equation 1. Figures 7(a) and 7(b) indicate that the average temperature of the air stream inside the collector is reduced when the scale is increased. In particular, the thickness of the thermal boundary layer normalized by the collector height is reduced as the scale is increased and the temperature gradient near the ground becomes larger, which is an indication of a higher heat transfer rate into the flow. However, this increased heat transfer is still not enough to result in a temperature as high as for the smaller collector. In summary, the air temperature rise underneath the collector is reduced for the larger scales.

Since the velocity in the chimney and the mass flow rate nevertheless become larger as the scale is increased, i.e., Figures 6(a) and 6(b), the conclusion must be drawn that this effect has to be attributed more to the increase in chimney height than to the temperature increase inside the collector. A higher heat transfer rate from the ground into the air stream inside the collector, e.g., through improved turbulence mixing, may increase the temperature at the chimney entrance section and, consequently, lead to a higher rising velocity in the tower and a larger available power.

Figure 8 provides an overview of the thermal efficiency of the collector for different scales. The collector efficiency increases significantly (more than 50%) when the scale is increased beyond 1:1 As discussed earlier, further improvements for larger scale plants are to be expected if the temperature rise underneath the collector could be increased.

The convective heat transfer into the ground was investigated as well. Radial distributions of the Nusselt number

$$Nu = \frac{hL}{K_{air}} \tag{6}$$

are shown in Figure 9. Here, h is the convective heat transfer coefficient, L is the reference length (here chosen as the collector gap size) and K_{air} is thermal conductivity of air. The Nusselt numbers rise with increasing scale. All curves indicate a sudden increase near the collector inlet ($r/R_c \sim 0.85$). This increase in the Nusselt number is likely associated with the turbulence model. In Figure 10 the wall-normal Reynolds stress component ($\overline{v'v'}$) at the collector mid-height is plotted versus the radial position. A comparison with Fig. 9 reveals that the turbulent fluctuations attain their maximum in the same region where the

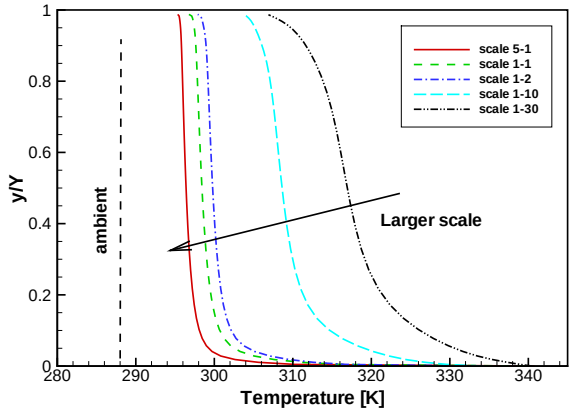

(a) Temperature distributions in the collector at $r = 3R_{chimney}$

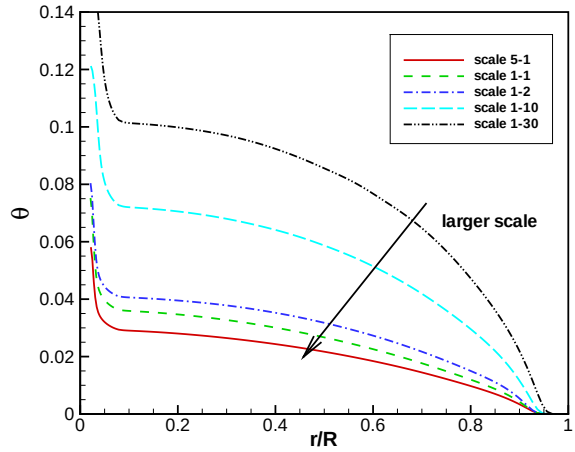

(b) Temperature distributions along the collector radius at collector mid-height

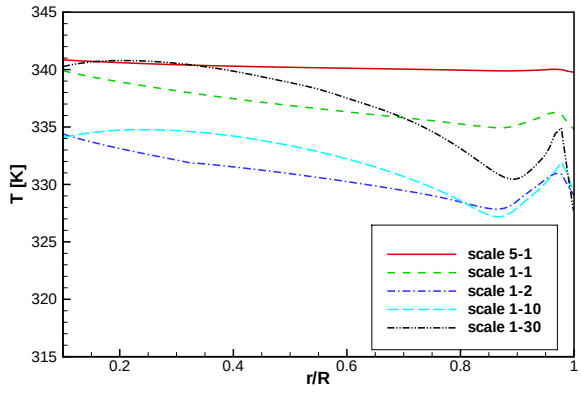

(c) Ground temperature calculated from energy balance model

FIGURE 7. Temperature distributions in the collector for different scales

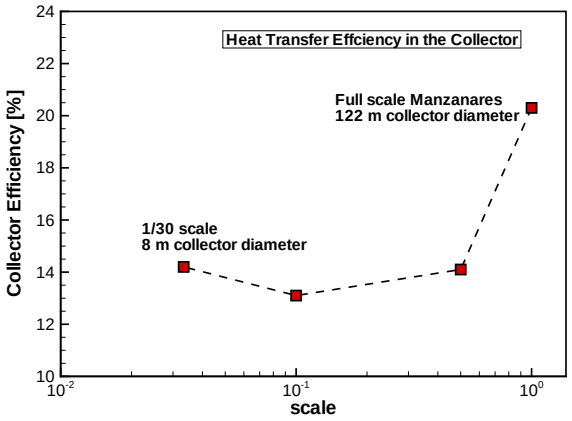

FIGURE 8. Thermal efficiency of the collector

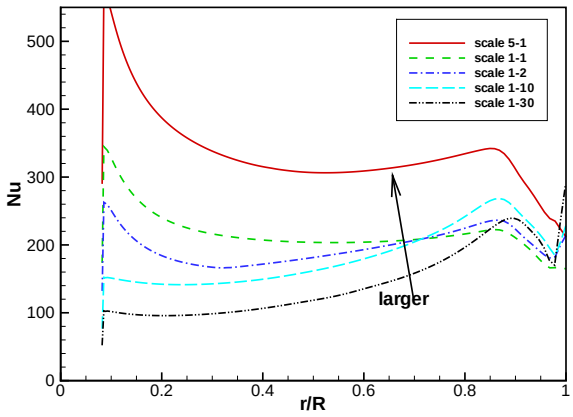

FIGURE 9. Nusselt number distributions on the ground in collector

Nusselt numbers are largest. Further investigations are required to clarify the role of the transition process from laminar to turbulent flow, which appears to be influenced by strong buoyancy effects in the low-speed section near the collector inlet. For example, Figure 11 shows contours of the axial velocity component for the collector region, where the increase in the Nusselt number occurs. Strong buoyancy forces and flow separation from the collector surface result in a flow recirculation, which appears to facilitate transition to turbulence.

The Reynolds number is an important parameter that has a strong influence on the flow behavior. The Reynolds number in the chimney based on chimney diameter,

$$Re_D = \frac{\rho v D}{\mu}, \tag{7}$$

varies between $Re_D = 10^4$ and 10^8 depending on the scale of the SCPP (Fig. 12(a)). The critical Reynolds number for pipe flow is 2000-10,000, depending on the wall roughness, and therefore the

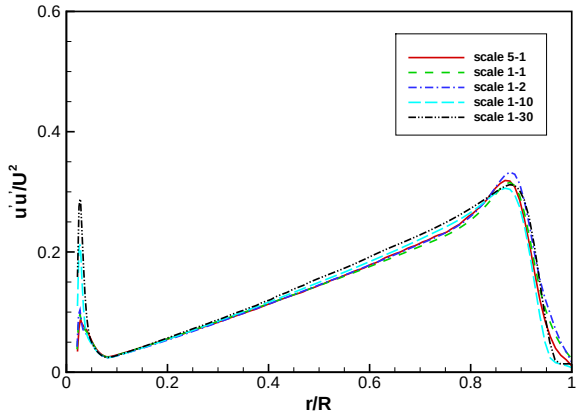

FIGURE 10. Wall-normal Reynolds stress distributions in collector

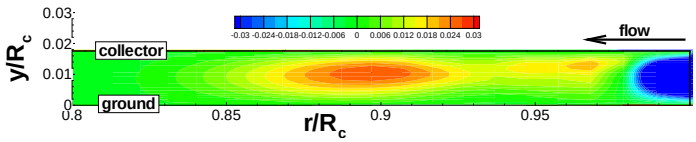

FIGURE 11. Flow recirculation near the collector inlet for Manzanares scale

flow in the chimney is expected to be turbulent for all scales considered here. The Reynolds number (based on collector height H) of the flow underneath the collector,

$$Re_h = \frac{\rho v H}{\mu}, \tag{8}$$

is plotted as a function of the radius in Fig. 12(b). For the small-scale models, transition to turbulence must be expected to take place further downstream of the collector inlet than for the larger scale models. To what extent the turbulence model in the CFD code can capture the exact transition location and what further actions have to be taken to improve the transition prediction remains subject of future research.

COLLECTOR GAP EFFECT

The collector height does not directly enter the simple formula for the power prediction (Eq. 2). Nevertheless, based on physical arguments it can be argued that the gap size should affect the temperature rise in the collector, the collector efficiency, and thus the mass flow rate. Practical considerations, such as ease of access and farming underneath the collector, may limit the minimum collector height. For this and other reasons, a detailed investigation of the effect of the collector height on the power will be of great practical value. An increased heat transfer from the ground into the air stream in the collector may be

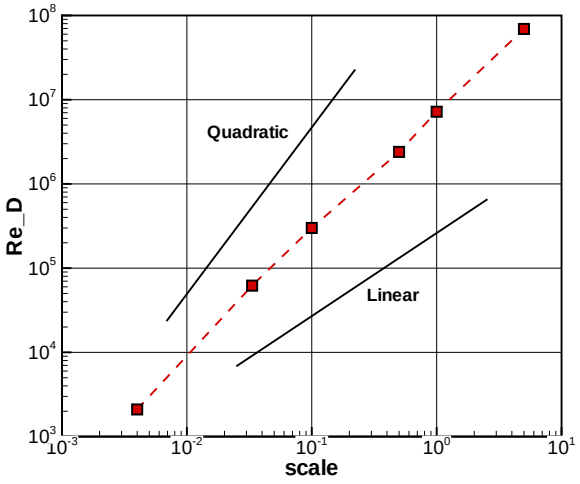

(a) Chimney

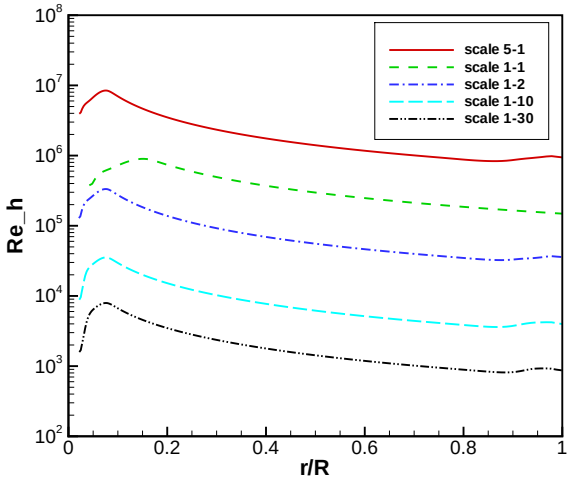

(b) Collector

FIGURE 12. Reynolds number distributions

achieved provided that the fluid dynamics in the collector were better understood. Pretorius (10) employed a one-dimensional computational model to show that the collector height had an effect on the performance of a solar chimney.

The effect of the collector height was investigated for the 1:30 and 1:1 scale plants. In Figure 13 the dependence of the power on the collector height is presented for these two cases. For the 1:30 scale model the optimum gap size is 0.6 times smaller than the reference collector height of the Manzanares plant, and for the 1:1 scale (Manazanares plant) the optimum gap size would be 0.9 times smaller. It should be mentioned that the designers of the Manzanares prototype plant were aware of the fact that the collector height was silghtly larger than its optimum value. It was intentionally made larger so that a small truck could be driven to the turbine section for maintenance purposes. For

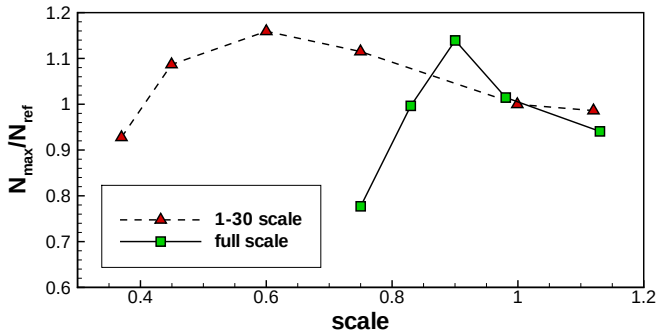

FIGURE 13. Effect of gap size on available power for two different scales

the proposed 200MW plants, the optimal collector height will already be large enough so that accessibility to the turbine will not be an issue. The present study indicates that the optimum collector height varies with the scale of the models, which is due to the different flow regimes (Reynolds numbers) for the different scale models.

SUMMARY AND CONCLUSION

Axisymmetric Unsteady Reynolds-Averaged Navier-Stokes (URANS) simulations were performed for Solar Chimneys Power Plants (SCPP) of different scales. The simulation approach was validated by comparison with data from the Manzanares prototype SCPP (which also served as a reference for the scaling) and a 1:250 scale laboratory model.

Overall, the present simulations confirm the cubic scaling of the available power with the plant dimensions as predicted by simple one-dimensional analysis (1). The temperature rise in the collector was shown to be inversely related to the scale of the plant. Nevertheless, the collector efficiency was found to increase considerably with increasing scale. The Reynolds numbers based on chimney diameter and collector height vary considerably with scale (from $Re_D = 10^4$ to 10^8 for the smallest and largest scale, respectively). Large variations were also observed for the Nusselt numbers associated with the heat transfer from the ground. A larger heat-transfer coefficient causes stronger buoyancy effects, which have a strong influence on the flow behavior underneath the collector. Laminar-turbulent transition was found to strongly affect the heat transfer in the collector, especially near the inlet section. Since no empirical transition correlation was employed, the laminar-turbulent transition location in the present calculations was dependent on the underlying RANS model. Additional research based on RANS models, that are tunned for transitional flow, or Direct Numerical Simulations (DNS) are required to better understand this phenomenon.

The effect of the collector height on the available power was

investigated to identify the optimum collector height for two different scaled models. The optima were found to be different for the two scales. Because of the large differences of the relevant Reynolds numbers, the difference in the optimum height likely results from the different flow regimes underneath the collector. In summary, the complex fluid dynamics in the collector strongly affect the temperature increase in the collector and hence the power output. Therefore, the flow behavior underneath the collector requires more detailed attention and will therefore be subject of future research. Towards this end, three-dimensional, unsteady high-resolution simulations for a 1:30 scale (Manzanares) model are planned, which will provide insight into the time-dependent fluid dynamics and heat transfer inside the collector. For the same scale, detailed experimental data will become available from a fully instrumented research plant that is currently being constructed at the University of Arizona. The experimental data from this plant will allow for additional verification and validation of the CFD Codes and simulation results.

Overall the present investigations confirm that CFD is a powerful tool for detailed analyses of Solar Chimney Power Plants.

ACKNOWLEDGMENT

The authors acknowledge support from the Arizona Research Institute for Solar Energy (AzRISE).

REFERENCES

[1] Schlaich, J., Bergermann, R., Schiel, W., and Weinrebe, G., 2005. "Design of Commercial Solar Updraft Tower Systems—Utilization of Solar Induced Convective Flows for Power Generation". *Journal of Solar Energy Engineering,* ***127***(1), Feb., pp. 117–124.

[2] dos Santos Bernardes, M., Molina Valle, R., and Cortez, M., 1999. "Numerical analysis of natural laminar convection in a radial solar heater". *International journal of thermal sciences,* ***38***(1), pp. 42–50.

[3] Bernardes, M., Voß, A., and Weinrebe, G., 2003. "Thermal and technical analyses of solar chimneys". *Solar Energy,* ***75***(6), p. 511.

[4] Pretorius, J. P., and Kröger, D. G., 2006. "Critical evaluation of solar chimney power plant performance". *Solar Energy,* ***80***(5), May, pp. 535–544.

[5] Haaf, W., Friedrich, K., Mayr, G., and Schlaich, J., 1983. "Solar chimneys part I: principle and construction of the pilot plant in Manzanares". *International Journal of Sustainable Energy,* ***2***(1), pp. 3–20.

[6] Shams, E., Gross, A., and Fasel, H., 2011. "Performance Analysis of Solar Chimneys of Different Physical Scales Using CFD". In Proceedings of the ASME Int. Conf. Energy Sustainability.

[7] Launder, B., and Spalding, D., 1974. "The numerical computation of turbulent flows". *Computer methods in applied mechanics and engineering,* ***3***(2), pp. 269–289.

[8] Ozisik, M., and Oezisik, M., 1993. *Heat conduction*, Vol. 8. John Wiley.

[9] Haaf, W., 1984. "Solar chimneys, part II: preliminary test results from the Manzanares pilot plant". *Int. J. Solar Energy,* ***2***, pp. 141–161.

[10] Pretorius, J., 2007. "Optimization and control of a large-scale solar chimney power plant". PhD thesis, Stellenbosch: University of Stellenbosch.